

ARTICLES

Electrochemical and Electronic Absorption Spectroscopic Studies of Substituent Effects in Iron(IV) and Manganese(IV) Corroles. Do the Compounds Feature High-Valent Metal Centers or Noninnocent Corrole Ligands? Implications for Peroxidase Compound I and II Intermediates**Erik Steene, Tebikie Wondimagegn, and Abhik Ghosh****Institute of Chemistry, Faculty of Science, University of Tromsø, N-9037 Tromsø, Norway**Received: May 30, 2001; In Final Form: September 13, 2001*

We report here an electrochemical and optical spectroscopic study of new Fe(IV) and Mn(IV) *meso*-triarylcorrole complexes. The complexes studied are three Fe(IV)Cl, three Mn(IV)Cl, and three dimeric Fe(IV)-OFe(IV) *meso*-tris(*p*-X-phenyl)corrole complexes, where X = CH₃, H, and CF₃. The first oxidation potentials of the Fe(IV)Cl and Mn(IV)Cl corrole complexes are considerably higher than those of the corresponding Fe(IV) corrole μ -oxo dimers, suggesting that the corrole ligands in the chloride complexes are already oxidized to a radical-like state. This is consistent with the suggestion by Walker and co-workers (ref 12) that the iron center in an (octaalkylcorrolato)Fe^{IV}Cl complex is best described as intermediate spin ($S = 3/2$) and that it is antiferromagnetically coupled to a corrole π -radical. We have attempted to clarify the nature of this antiferromagnetic coupling by means of DFT calculations and propose that it results from an metal(d_{z^2})-corrole("b₁") orbital interaction. In contrast, the corrole ligand in the Fe(IV) corrole μ -oxo dimers does not seem to have radical character. The optical spectra of the Fe(IV)Cl and Mn(IV)Cl corrole derivatives exhibit distinctive split Soret bands, one arm of which is strongly substituent sensitive. This behavior contrasts with that of free-base corroles and porphyrins and of typical metalloporphyrins whose optical spectra are relatively substituent-insensitive. We qualitatively assign this substituent-sensitive feature to a transition with significant ligand-to-metal charge-transfer character.

Introduction

Iron(IV) complexes have been detected or proposed as reactive intermediates for various heme and nonheme iron enzymes, as well as for a number of synthetic biomimetic model systems.¹ A wide variety of spectroscopic techniques have been used to probe the geometric and electronic structures of enzymatic and synthetic iron(IV) intermediates. A key point of interest in these studies has involved the question of where the oxidation equivalents reside in these high-valent molecules, i.e., whether these species are oxidized in a metal- or ligand-centered fashion, relative to analogous lower-valent complexes. Recent theoretical studies² have contributed to a greatly enhanced understanding of the factors that result in this rich electronic-structural diversity among compound I intermediates. Developments in corrole chemistry suggest that a similar diversity of electronic structures might emerge for iron^{3,4} and manganese^{4,5} corroles. From a practical standpoint, high-valent metalcorroles^{3,4} are also of particular interest because of their relative stability and ease of handling and characterization.

We report here the preparation, optical spectra, and an electrochemical study of new iron(IV) and manganese(IV) *meso*-triarylcorroles with different *para*-substituents (CH₃, H, and CF₃)

on the *meso* phenyl groups (Figure 1). In addition, we report preliminary DFT calculations on unsubstituted model compounds (corrolato)Fe^{IV}X and (corrolato)Mn^{IV}X (X = Cl, OLi). The combined electrochemical and theoretical results afford significant insights into the nature of the formally high-valent iron and manganese centers, the issue of ligand noninnocence, and substituent effects on the electronic character of these high-valent complexes.⁶

Methods. Free-base *meso*-triarylcorroles with the *para*-substituents CH₃, H, and CF₃ were synthesized from pyrrole and the relevant *para*-substituted benzaldehydes by a straightforward application of the procedure reported by Gross and co-workers for tris(pentafluorophenyl)corrole, H₃TPFPC.⁷ Although the procedure described in ref 7 specifically refers to electron-deficient aromatic aldehydes, we found that it worked for a broad range of aldehydes. The free-base corroles were exhaustively characterized by spectroscopic methods and elemental analysis.⁸ Iron was inserted into these ligands via the interaction of the free-base corroles with Fe₂(CO)₉ in refluxing toluene, exactly as described by Vogel et al. for octaethylcorrole.³ After aerial oxidation, this reaction gave the Fe(IV) μ -oxo dimer derivatives of the corroles. Monomeric Fe(IV) chloride complexes were prepared from the μ -oxo dimers by treatment with dilute aqueous HCl, as described by Vogel et al.³ Manganese was inserted into the corroles by reaction with Mn(OAc)₂•4H₂O

* To whom correspondence should be addressed. E-mail: abhik@chem.uit.no. Fax: +47 7764 4072.

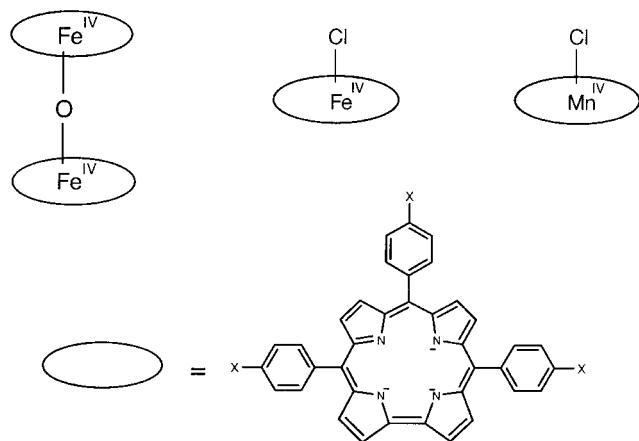


Figure 1. Compounds studied in this work; X = CH₃, H, and CF₃.

in refluxing DMF. Elemental analyses and MALDI-TOF mass spectra of all compounds prepared were as expected on the basis of the molecular formulas. Proton NMR (CDCl₃, room temperature) data for the iron compounds, along with proposed assignments, and UV-vis absorption spectroscopic data (in dichloromethane) are as follows. The NMR spectra and a discussion of the proposed assignments are given in the Supporting Information. The Mn(IV) Cl corrole complexes gave rise to broad, paramagnetically shifted peaks in the proton NMR spectra, which have not yet been assigned.

(T(p-CF₃-P)C)Fe^{IV}Cl. ¹H NMR: 24.0 (s, 2H, β-pyrrolic), 22.8 (s, 2H, β-pyrrolic), 22.0 (s, 2H, β-pyrrolic), 5.55 (s, 2H, β-pyrrolic or *o*-phenyl), -1.75 (s, 2H, *m*-phenyl), -1.95 (s, 2H *m*-phenyl), -2.77 (s, 1H *m*-phenyl), -2.87 (s, 1H *m*-phenyl), -6.29 (s, 2H, *o*-phenyl), -6.78 (s, 2H, *o*-phenyl), -39.8 (s, 2 H, β-pyrrolic or *o*-phenyl). λ_{max} (log ε/(M⁻¹cm⁻¹)): 366 nm (4.60), 402 nm (4.72).

(TPC)Fe^{IV}Cl. ¹H NMR: 25.2 (s, 2H, β-pyrrolic), 24.0 (s, 2H, β-pyrrolic), 23.1 (s, 2H, β-pyrrolic), 19.6 (s, 2H, *p*-phenyl), 17.2 (s, 1H, *p*-phenyl), 6.01 (s, 2H, β-pyrrolic or *o*-phenyl), -2.56 (s, 2H, *m*-phenyl), -2.85 (s, 2H, *m*-phenyl), -3.71 (s, 1H, *m*-phenyl), -3.91 (s, 1H, *m*-phenyl), -5.79 (s, 2H, *o*-phenyl), -6.94 (s, 2H, *o*-phenyl), -41.1 (s, 2H, β-pyrrolic or *o*-phenyl?). λ_{max} (log ε/(M⁻¹cm⁻¹)): 359 nm (4.53), 411 nm (4.63).

(T(p-CH₃-P)C)Fe^{IV}Cl. ¹H NMR: 26.0 (s, 2H, β-pyrrolic), 24.7 (s, 2H, β-pyrrolic), 23.9 (s, 2H, β-pyrrolic), 5.75 (s, 2H, β-pyrrolic or *o*-phenyl), -3.23 (s, 2H, *m*-phenyl), -3.38 (s, 2H, *m*-phenyl), -4.51 (s, 1H, *m*-phenyl), -4.67 (s, 1H, *m*-phenyl), -5.41 (s, 2H, *o*-phenyl), -7.25 (s, 2H, *o*-phenyl), -9.61 (s, 3H, *p*-CH₃), -11.9 (s, 6H, *p*-CH₃), -41.4 (s, 2H, β-pyrrolic or *o*-phenyl). λ_{max} (log ε/(M⁻¹cm⁻¹)): 361 nm (4.60), 421 nm (4.61).

[(T(p-CF₃-P)C)Fe^{IV}]₂O. ¹H NMR: 7.71–7.77 (m, 10H, phenyl), 7.64 (d, *J* = 6.7 Hz, 4H, phenyl), 7.59 (d, *J* = 7.3 Hz, 2H, phenyl), 7.52 (d, *J* = 7.3, 6H,⁹ phenyl), 7.35 (d, *J* = 4.3 Hz, 4H, β-pyrrolic), 7.24 (d, *J* = 4.9 Hz, 4H, β-pyrrolic), 7.11 (d, *J* = 7.9 Hz, 2H, phenyl), 6.94 (d, *J* = 4.3 Hz, 4H, β-pyrrolic), 6.76 (d, *J* = 4.9 Hz, 4H, β-pyrrolic). λ_{max} (log ε/(M⁻¹cm⁻¹)): 384 nm (5.03).

[(TPC)Fe^{IV}]₂O. ¹H NMR: 7.61 (s, 4H, phenyl), 7.37–7.54 (m, 22H, phenyl and β-pyrrolic), 7.29 (m, 8H, phenyl and/or β-pyrrolic), 7.25 (d, *J* = 7.3 Hz, 2H, phenyl), 7.11 (d, *J* = 7.3 Hz, 2H, phenyl), 7.00 (d, *J* = 4.9 Hz, 4H, β-pyrrolic), 6.83 (d, *J* = 4.9 Hz, 4H, β-pyrrolic). λ_{max} (log ε/(M⁻¹cm⁻¹)): 385 nm (5.09).

[(T(p-CH₃-P)C)Fe^{IV}]₂O. ¹H NMR: 7.29–7.49 (m, 26H, phenyl and/or β-pyrrolic), 7.21 (m, 4H, phenyl and/or β-pyr-

TABLE 1: Half-Wave Potentials (V vs SCE) for [Fe^{IV}T(p-X-P)C]Cl, [Fe^{IV}T(p-X-P)C]₂O, and [Mn^{IV}T(p-X-P)C]Cl (X = CH₃, H, CF₃) in CH₂Cl₂ Containing 0.1 M TBAP^a

corrole	X	3σ	E _{1/2ox}	E _{1/2red}
Fe ^{IV} [T(p-X-P)C]Cl	CH ₃	-0.51	1.015	0.033
	H	0	1.068	0.050
	CF ₃	1.62	1.178	0.190
[Fe ^{IV} T(p-X-P)C] ₂ O	CH ₃	-0.51	0.593	-0.350
	H	0	0.635	-0.305
	CF ₃	1.62	0.830	-0.115
Mn ^{IV} [T(p-X-P)C]Cl	CH ₃	-0.51	0.970	0.072
	H	0	1.032	0.093
	CF ₃	1.62	1.150	0.230

^a A scan rate of 0.1 Vs⁻¹ was used. See also Figures 2, 3, and 4 for additional redox potential data.

rolic), 7.09 (d, *J* = 6.9 Hz, 2H, phenyl), 7.03 (d, *J* = 4.5 Hz, 4H, phenyl and/or β-pyrrolic), 6.84 (d, *J* = 4.5 Hz, 4H, phenyl and/or β-pyrrolic), 2.51 (s, 12H, *p*-CH₃), 2.46 (s, 6H, *p*-CH₃). λ_{max} (log ε/(M⁻¹cm⁻¹)): 389 nm (4.94).

(T(p-CF₃-P)C)Mn^{IV}Cl. λ_{max} (log ε/(M⁻¹cm⁻¹)): 316 (4.32), 364 (4.40), 423 nm (4.62).

(TPC)Mn^{IV}Cl. λ_{max} (log ε/(M⁻¹cm⁻¹)): 314 (4.37), 358 (4.44), 433 nm (4.66).

(T(p-CH₃-P)C)Mn^{IV}Cl. λ_{max} (log ε/(M⁻¹cm⁻¹)): 319 (4.40), 363 (4.47), 443 nm (4.64).

Cyclic voltammetry was carried out using an EG&G Model 263A Potentiostat with a three-electrode system consisting of a glassy carbon working electrode, a platinum wire counter-electrode and a saturated calomel reference electrode (SCE). Tetra(*n*-butyl)ammonium perchlorate (TBAP) recrystallized from ethanol and dried in a vacuum for at least one week was used as supporting electrolyte. Dichloromethane, distilled and kept over molecular sieves, was used as solvent. The reference electrode was separated from bulk solution by a fritted-glass bridge filled with the solvent/supporting electrolyte mixture, and all potentials were referenced to the SCE. Pure nitrogen was bubbled through solutions containing the metalcorroles for at least 2 min prior to running the experiments and the solutions were also protected from air by a nitrogen blanket during the experiment.

DFT calculations on (corrolato)MX complexes (M = Fe, Mn; X = Cl, OLi) were carried out using Slater-type valence triple-ζ plus polarization basis sets, the VWN local functional, the Perdew-Wang 1991 gradient corrections, a spin-unrestricted formalism, a fine mesh for numerical integration of matrix elements, full geometry optimizations with C_s symmetry constraints, and the ADF¹⁰ program system.

Electrochemical Results. Table 1 presents the oxidation and reduction potential data for the iron and manganese corroles prepared. The corresponding cyclic voltammograms are shown in Figure 2, 3, and 4. Figure 5, 6, and 7 shows Hammett plots for the redox potentials of the Fe(IV) corrole chloride, the Fe(IV) corrole μ-oxo dimer, and the Mn(IV) corrole chloride series, respectively.

The oxidation potentials of the Fe(IV) corrole chloride complexes are considerably higher than those of the corresponding Fe(IV) corrole μ-oxo dimers. This suggests that the nature of the one-electron oxidation is different in the two families of compounds. The oxidation potentials of the Fe(IV) corrole μ-oxo dimers are comparable to those observed for the corresponding Cu(III) corroles (e.g., E_{1/2ox} (Cu^{III}TPC) = 0.76 V vs SCE).¹¹ Because the electrochemical generation of Cu(IV) and Fe(V) corroles is unlikely, we propose that the Fe(IV)

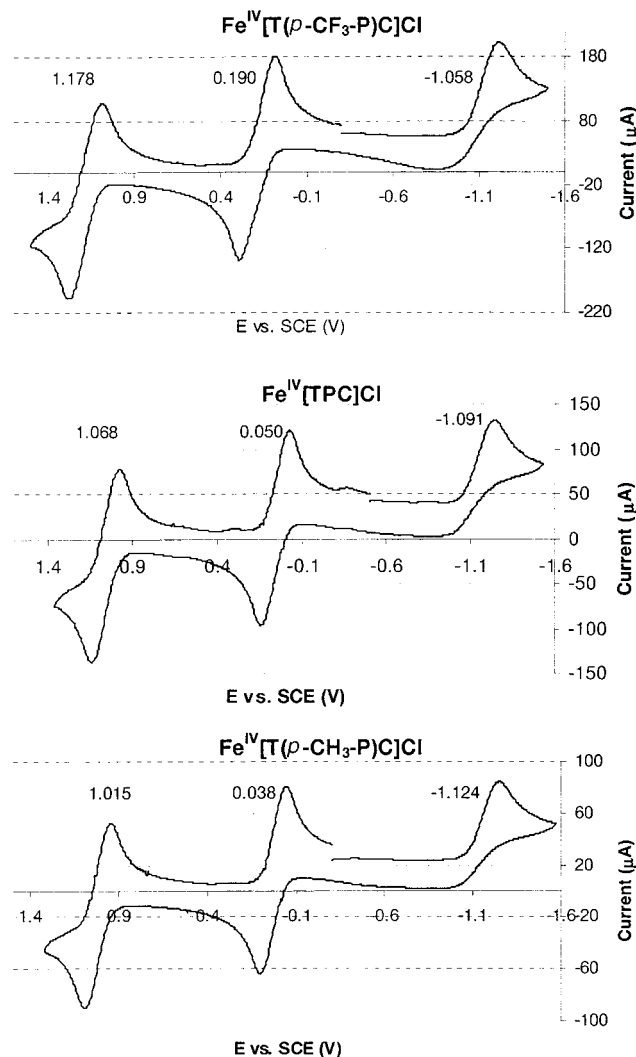


Figure 2. Cyclic voltammograms of Fe^{IV}[T(*p*-X-P)C]Cl (X = CH₃, H, CF₃) in CH₂Cl₂ with TBAP as the supporting electrolyte. The various redox potentials are indicated.

corrole μ -oxo dimers undergo ligand-centered oxidation. The significantly higher oxidation potentials for the Fe(IV) corrole chloride complexes suggests that the corrole ligand in these complexes is already oxidized and that the electrochemical one-electron oxidation is at least significantly metal-centered. This is consistent with the proposal by Walker et al. that Fe^{IV}(OMC)-Cl (OMC = β -octamethylcorrole) is better described as intermediate-spin Fe(III) antiferromagnetically coupled to an OMC "cation" radical.¹² However, based on spectroelectrochemical measurements, Gross and co-workers have suggested that one-electron oxidation and reduction of Fe^{IV}(TPFPC)Cl are corrole- and metal-centered, respectively.^{4c} Thus, Gross and co-workers have favored a clean Fe(IV) description for Fe^{IV}(TPFPC)Cl.

The electrochemical results show that substituents at the *para*-positions of the *meso*-phenyl groups exert significant effects on the oxidation and reduction potentials. The observed ρ -values ($\rho = 1/3 dE_{1/2}/d\sigma$) are 74 mV for the first oxidation of the Fe(IV) corrole chloride series, 77 mV for the first reduction of this series, 114 mV for the first oxidation of the Fe(IV) corrole μ -oxo dimer series, and 109 mV for the first reduction of this series. These ρ -values are comparable to those found for corresponding metallotetraphenylporphyrins¹³ where ($\rho = 1/4 dE_{1/2}/d\sigma$). The relatively high ρ -values for oxidation, comparable to the ones found for metallotetraphenylporphyrins, are consistent with an

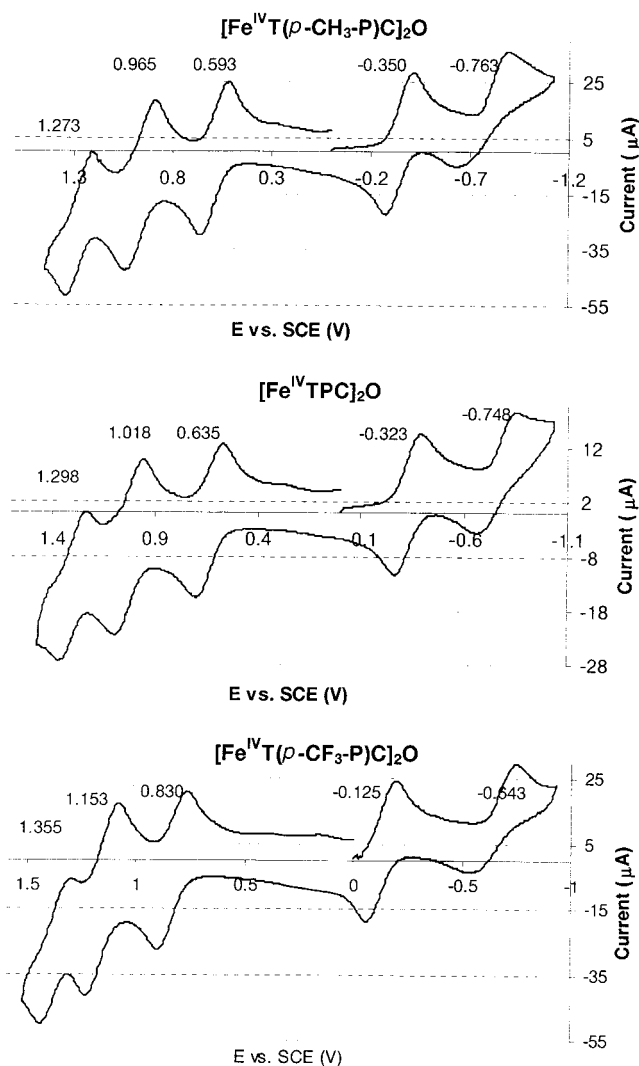


Figure 3. Cyclic voltammograms of [Fe^{IV}T(*p*-X-P)C]₂O (X = CH₃, H, CF₃) in CH₂Cl₂ with TBAP as the supporting electrolyte. The various redox potentials are indicated.

oxidation from the a_{2u} -like b_1 HOMO that has considerable electron density at the *meso*-positions (see Figure 8).¹⁴

The ρ -values for oxidation and reduction in the Fe(IV) corrole μ -oxo dimer series are significantly higher than for the corresponding Fe(IV) corrole chloride series. This suggests that the oxidation and reduction equivalents in the former series of compounds are distributed in such a manner that they sense the substituent effects of more than three *meso*-aryl substituents.

DFT Calculations. Spin-unrestricted DFT calculations on (corrolato)Fe^{IV}Cl and (corrolato)Mn^{IV}Cl reveal rather complex spin density profiles (Figure 9). Thus, for (corrolato)Fe^{IV}Cl, the Fe and Cl atoms carry 2.00 and 0.22 α spins and the β -carbons carry a total of 0.10 α spins. In contrast, the *meso* carbons carry a total of 0.28 β spins and the nitrogens carry 0.14 β spins. For (corrolato)Mn^{IV}Cl, the Mn and Cl atoms carry 3.22 and 0.14 α spins and the β -carbons carry a total of 0.087 α spins. In contrast, the *meso* carbons carry a total of 0.30 β spins and the nitrogens carry 0.29 β spins. This spatial distribution of the β spins in these two M(IV)Cl complexes coincides precisely with the shape of the b_1 HOMO of the corrole ligand, which crudely resembles the a_{2u} HOMO of porphyrins. The overall spin density profiles of these molecules, in particular, the significant spatial separation of the α and β spins, are highly characteristic of antiferromagnetically coupled spin systems.^{6d} In this case, the

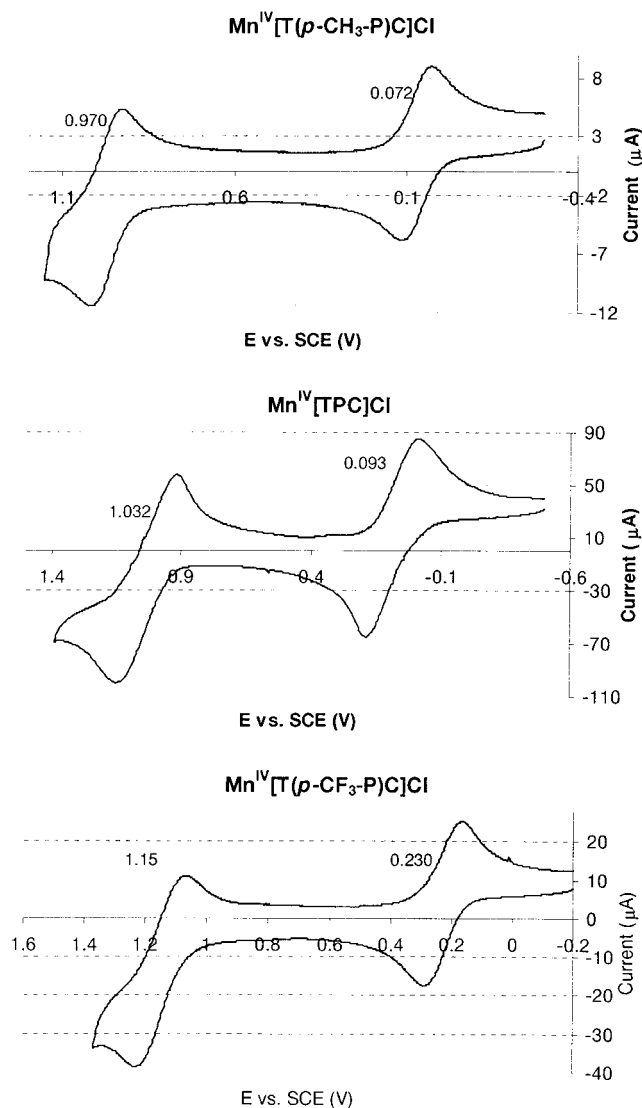


Figure 4. Cyclic voltammograms of $\text{Mn}^{\text{IV}}[\text{T}(p\text{-X-P})\text{C}]\text{Cl}$ ($X = \text{CH}_3, \text{H}, \text{CF}_3$) in CH_2Cl_2 with TBAP as the supporting electrolyte. The various redox potentials are indicated.

antiferromagnetic coupling seems to involve the metal center on the one hand and the corrole b_1 HOMO on the other hand. An examination of the high-lying occupied MOs of each of these molecules revealed an MO with an metal(d_{z^2})-corrole (“ b_1 ”) overlap. This overlap is clearly facilitated by the significant displacement of 0.4–0.5 Å of the metal atom from the N_4 plane of the corrole in the optimized geometry of (corrolato) $\text{M}^{\text{IV}}\text{Cl}$, which is in good agreement with a displacement of 0.422 Å in the X-ray crystal structure of (OEC) $\text{Fe}^{\text{IV}}\text{Cl}$.³ The $\text{Fe}(d_{z^2})$ -corrole (“ b_1 ”) overlap revealed by our calculations is consistent with the suggestion by Walker and co-workers that the iron center is best described as intermediate spin ($S = 3/2$) and that it is antiferromagnetically coupled to a corrole π -radical.¹² In the same way, we propose that the electronic structures of (corrolato) $\text{Mn}^{\text{IV}}\text{Cl}$ has some significant $S = 2$ Mn(III) character, with antiferromagnetic coupling to a corrole b_1 radical.

An analogous electronic-structural scenario has been proposed for five-coordinate high-spin iron(III) porphyrin π -cation radicals such as $[(\text{OEP})\text{FeCl}]^+$ and $[(\text{OEP})\text{FeBr}]^+$.¹⁵ Structural, Mössbauer,¹⁵ and theoretical^{6d} studies on these and related compounds indicate that the d_{z^2} electron of the high-spin iron(III) center is antiferromagnetically coupled to a porphyrin a_{2u} radical, leading to an overall $S = 2$ spin state.

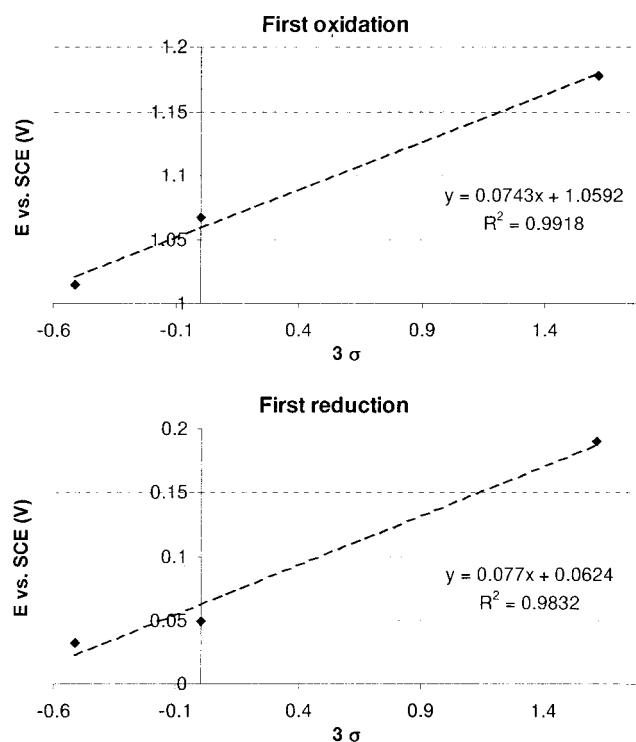


Figure 5. Hammett plots for the first oxidation and reduction of the $\text{Fe}^{\text{IV}}[\text{T}(p\text{-X-P})\text{C}]\text{Cl}$ series ($X = \text{CH}_3, \text{H}, \text{CF}_3$).

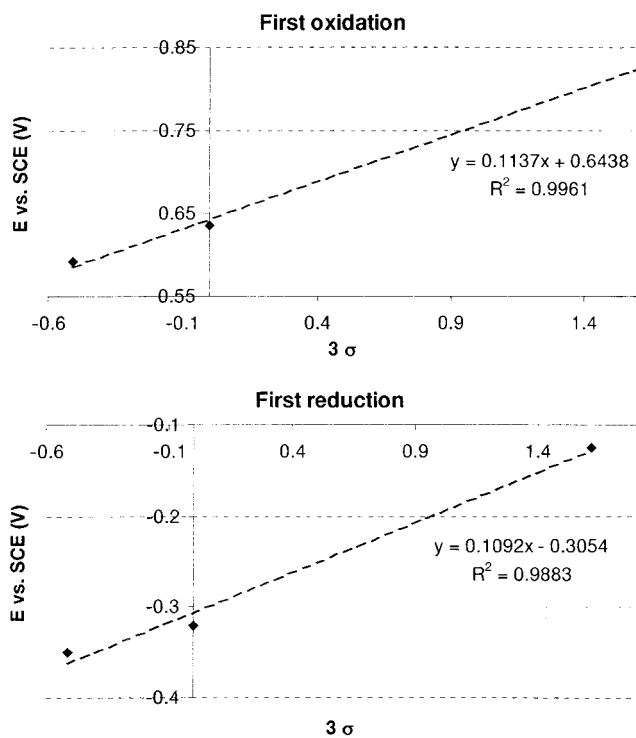


Figure 6. Hammett plots for the first oxidation and reduction of the $[\text{Fe}^{\text{IV}}\text{T}(p\text{-X-P})\text{C}]_2\text{O}$ series ($X = \text{CH}_3, \text{H}, \text{CF}_3$).

Obviously, the spatial separation of the α and β spins does not correspond to any real spin density profile but is an artifact of the spin-unrestricted DFT method. A proper description of antiferromagnetic coupling is better achieved via traditional ab initio methods such as multiconfigurational SCF calculations, but we have not yet accomplished such calculations on the large molecules of interest in this study, although a modest beginning has been made.^{6d}

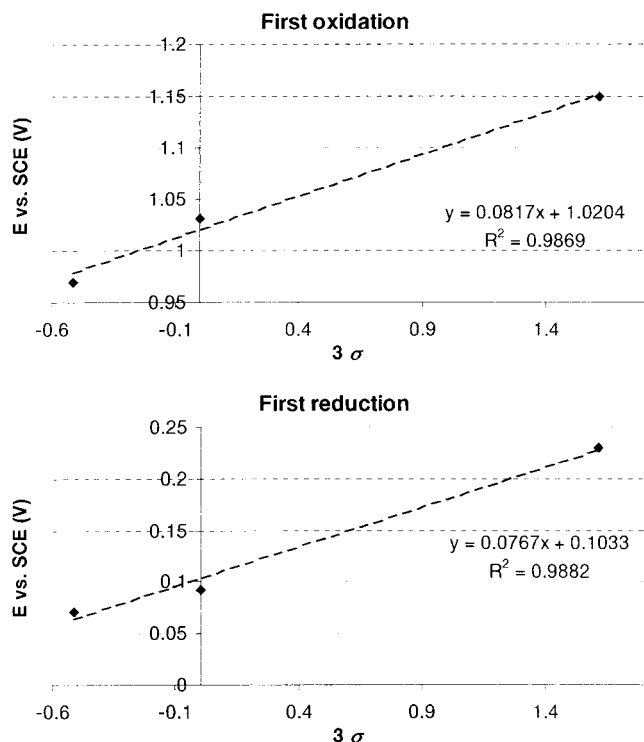


Figure 7. Hammett plots for the first oxidation and reduction of the $\text{Mn}^{\text{IV}}[\text{T}(p\text{-X-P})\text{C}]\text{Cl}$ series ($\text{X} = \text{CH}_3, \text{H}, \text{CF}_3$).

In contrast to the rather complex spin density profile of $(\text{corrolato})\text{Fe}^{\text{IV}}\text{Cl}$, a DFT calculation on $(\text{corrolato})\text{Fe}^{\text{IV}}\text{OLi}$ shows that the unpaired spin density is entirely localized on the Fe–O unit, with the atomic spin populations being 1.2 for Fe and 0.82 for O. This result shows that with a strongly basic axial ligand such as oxide, the corrole ligand does not have radical character. This parallels a similar lack of unpaired spin density on the porphyrin ring of peroxidase compound II and synthetic Fe(IV)-oxo model systems. These calculations provide an explanation for the considerably lower oxidation potentials of the Fe(IV) corrole μ -oxo dimers relative to the corresponding Fe(IV) corrole chloride complexes. These calculated electronic structural descriptions are also consistent with the significantly lower Mössbauer isomer shift for $[(\text{OEC})\text{Fe}]_2\text{O}$ (0.02 mm/s) relative to $(\text{OEC})\text{FeCl}$ (0.19 mm/s).³

Optical Spectra. The optical spectra of the Fe(IV) and Mn(IV) corrole chloride derivatives (Figures 10 and 12 respectively) exhibit highly distinctive split Soret bands, one arm of

which is strongly substituent sensitive, as shown in Table 2. This strong sensitivity may be contrasted with the relative invariance of the absorption spectra of free-base triarylcorroles as well as of free-base and metallotetraarylporphyrins as a function of substituents in the *para*-position of the phenyl rings.¹³ We propose that the substituent sensitive band in the absorption spectra of the Fe(IV) and Mn(IV) corrole chloride complexes have significant ligand-to-metal charge-transfer character. Interestingly, the optical spectra of the Fe(IV) corrole μ -oxo dimers studied do not exhibit similarly large substituent effects. The reason for this difference in behavior of the Fe(IV) corrole chlorides and the Fe(IV) corrole μ -oxo dimers is not clear at present.

Note also that the optical spectra of the Fe(IV) and Mn(IV) corrole chloride complexes are considerably red-shifted and exhibit “hyperporphyrin” character, relative to those of the Fe(IV) corrole μ -oxo dimers. This is somewhat of a novelty compared to Fe(IV)-oxo porphyrins such as peroxidase compound II intermediates and their synthetic models. However, chloroperoxidase compound II (CPO–II) also exhibits a hyper spectrum, with a split Soret band with maxima at 373 and 436 nm; in addition, according to Egawa et al., “Resonance enhancement of the $\nu_{\text{Fe}=\text{O}}$ stretching (ν_{FeO}) Raman band was found for CPO–I^{16c} when Raman scattering was excited at wavelengths within both transition bands around 365 and 415 nm, whereas the ν_{FeO} Raman band was not identified for CPO–II at any of the excitation wavelengths examined”.¹⁷ On the basis of our own results on $\text{Fe}^{\text{IV}}\text{Cl}$ and Fe^{IV} -oxo corroles and those of Egawa et al.,¹⁶ it may even be reasonable to totally reconsider the molecular and electronic structure of CPO–II: It is possible that CPO–II may not be a high-valent iron-oxo intermediate! Instead, the putative oxo group in CPO–II may actually be protonated, i.e., an OH group. An OH group, like the axial Cl ligand in our $\text{Fe}^{\text{IV}}\text{Cl}$ corroles, would be less able to stabilize a high-valent iron center than a terminal oxo ligand, which would also be consistent with the hyperporphyrin character of CPO–II.¹⁶

Resonance Raman Spectra (note added in proof): Since the initial submission of this paper, we have succeeded in obtaining the resonance Raman (RR) spectra of the Mn(IV) and Fe(IV) corroles reported in this paper (Figure 13) using a Spex Jobin–Yvon double monochromator equipped with a liquid nitrogen cooled Spex Jobin–Yvon CCD 2000 detector and the 457.9 nm laser line of a Coherent Innova 70 Series mixed Ar–Kr laser. We had hoped that the RR spectra would provide valuable insights into differences in the electronic character of the corrole ligand among the different compounds. Unfortu-

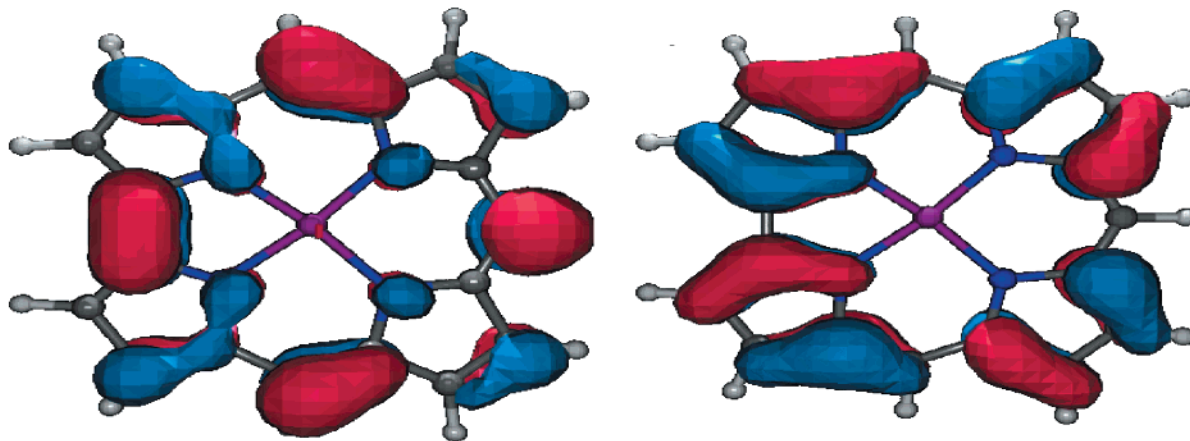


Figure 8. The b_1 and a_2 HOMOs of Ga(III) corrole, chosen as a representative closed-shell metallocorrole.

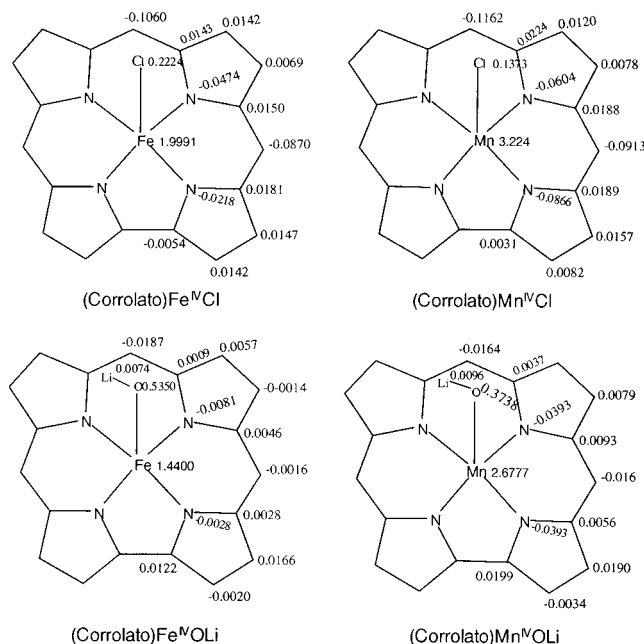


Figure 9. Calculated gross atomic spin populations obtained from spin-unrestricted DFT calculations.

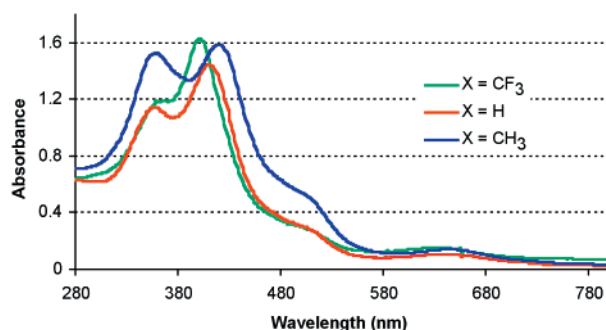


Figure 10. UV-vis absorption spectra of $\text{Fe}^{\text{IV}}[\text{T}(p\text{-X-P})\text{C}]\text{Cl}$.

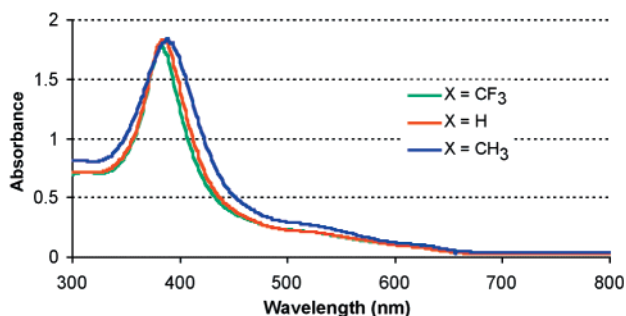


Figure 11. UV-vis absorption spectra of $\text{Fe}^{\text{IV}}[\text{T}(p\text{-X-P})\text{C}]_2\text{O}$.

nately, the spectra do not exhibit many readily interpretable trends. Nevertheless, a few preliminary observations may be made, albeit at a rather descriptive level. For example, the band at 1533 cm^{-1} in the RR spectrum of $\text{Fe}^{\text{IV}}[\text{T}(p\text{-CF}_3\text{-P})\text{C}]\text{Cl}$ downshifts to 1527 and 1529 cm^{-1} for $\text{Fe}^{\text{IV}}[\text{T}(p\text{-CH}_3\text{-P})\text{C}]\text{Cl}$ and $\text{Fe}^{\text{IV}}[\text{TPC}]\text{Cl}$, respectively. Similarly, the band at 1528 cm^{-1} for $\text{Mn}^{\text{IV}}[\text{T}(p\text{-CF}_3\text{-P})\text{C}]\text{Cl}$ downshifts to 1517 and 1521 cm^{-1} for $\text{Mn}^{\text{IV}}[\text{T}(p\text{-CH}_3\text{-P})\text{C}]\text{Cl}$ and $\text{Mn}^{\text{IV}}[\text{TPC}]\text{Cl}$, respectively. These results may indicate that the electronic character of the corrole ligand in the $\text{M}^{\text{IV}}[\text{T}(p\text{-CF}_3\text{-P})\text{C}]\text{Cl}$ ($\text{M} = \text{Fe}, \text{Mn}$) derivatives may be significantly different, perhaps with respect to radical character, relative to the analogous derivatives involving the more electron-rich TPC and $\text{T}(p\text{-CH}_3\text{-P})\text{C}$ ligands.

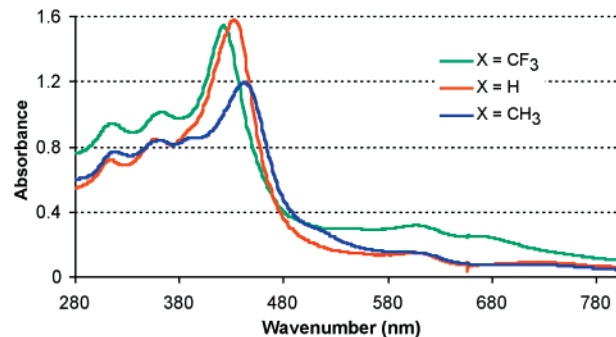


Figure 12. UV-vis absorption spectra of $\text{Mn}^{\text{IV}}[\text{T}(p\text{-X-P})\text{C}]\text{Cl}$.

TABLE 2: “Soret” Band Maxima (nm) in CH_2Cl_2 for the Fe(IV) and Mn(IV) Triarylcorroles Studied

corrole	<i>para</i> -substituent (X)		
	CH_3	H	CF_3
$\text{Fe}^{\text{IV}}[\text{T}(p\text{-X-P})\text{C}]\text{Cl}$	361, 421	359, 411	366, 402
$[\text{Fe}^{\text{IV}}\text{T}(p\text{-X-P})\text{C}]_2\text{O}$	389	385	384
$\text{Mn}^{\text{IV}}[\text{T}(p\text{-X-P})\text{C}]\text{Cl}$	319, 363, 443	314, 358, 433	316, 364, 423

^a The highly substituent-sensitive bands are marked in bold.

Further, certain peaks in the Fe(IV)Cl corrole complexes appear to be modestly upshifted in the corresponding Fe(IV)–O–Fe(IV) derivatives. For instance, the bands at 1533 and 1494 cm^{-1} for $\text{Fe}^{\text{IV}}[\text{T}(p\text{-CF}_3\text{-P})\text{C}]\text{Cl}$ appear to upshift to 1537 and 1499 cm^{-1} , respectively, for $\{\text{Fe}^{\text{IV}}[\text{T}(p\text{-CF}_3\text{-P})\text{C}]\}_2\text{O}$. Similarly, the bands at 1527 , 1485 , and 1499 cm^{-1} for $\text{Fe}^{\text{IV}}[\text{TPC}]\text{Cl}$ appear to upshift to 1534 , 1489 , and 1503 cm^{-1} , respectively, for $\{\text{Fe}^{\text{IV}}[\text{TPC}]\}_2\text{O}$, and the bands at 1529 and 1489 cm^{-1} for $\text{Fe}^{\text{IV}}[\text{T}(p\text{-CH}_3\text{-P})\text{C}]\text{Cl}$ appear to upshift to 1532 and 1495 cm^{-1} , respectively, for $\{\text{Fe}^{\text{IV}}[\text{T}(p\text{-CH}_3\text{-P})\text{C}]\}_2\text{O}$. These upshifts may be indicative of a systematic difference in electronic character of the corrole ligand between the Fe(IV)Cl versus Fe(IV)–O–Fe(IV) derivatives, as discussed elsewhere in the paper.

Ongoing experimental work in our laboratory include temperature-dependent NMR studies of the paramagnetic Fe(IV) corrole chloride complexes as well as Mössbauer spectroscopy of all the iron(IV) corroles reported herein.

Conclusions

The following are some of the key conclusions of this study.

1. The observed variations in redox potentials among the different Fe(IV) and Mn(IV) complexes studied indicate that *meso*-aryl substituents can strongly modulate the electronic nature of metallocorrole complexes.

2. The first oxidation potentials of the Fe(IV) corrole chloride complexes are considerably higher than those of the corresponding Fe(IV) corrole μ -oxo dimers, suggesting that the corrole ligands in the former complexes are already oxidized to a radical-like state. This is consistent with the suggestion by Walker and co-workers that the iron center is best described as intermediate spin ($S = 3/2$) and that it is antiferromagnetically coupled to a corrole π -radical. DFT calculations have clarified the nature of this antiferromagnetic coupling and attribute it to an $\text{Fe}(d_{z^2})$ -corrole(“ b_1 ”) orbital interaction. In contrast, the corrole ligand in the Fe(IV) corrole μ -oxo dimers does not seem to have radical character. The RR spectra, although not analyzed in detail, may also be consistent with the conclusions.

3. The first oxidation potentials of the Mn(IV) corrole chloride complexes are approximately the same as those for the analogous Fe(IV)Cl complexes.

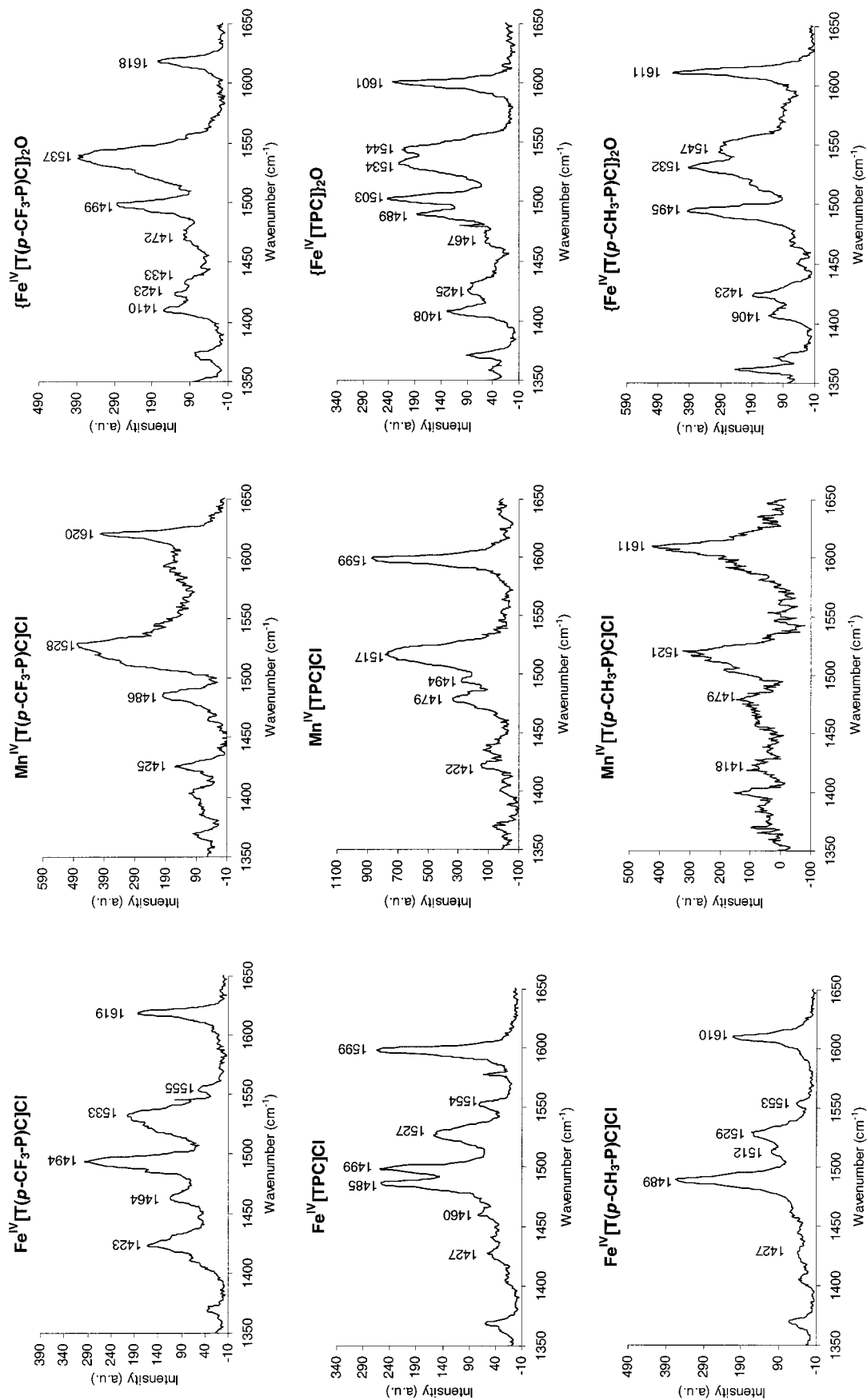


Figure 13. Resonance Raman spectra ($\lambda_{\text{ex}} = 457.9$ nm) of the Fe(IV) and Mn(IV) corroles studied.

4. The optical spectra of the Fe(IV) and Mn(IV) corrole chloride derivatives exhibit distinctive split Soret bands, one

arm of which is strongly substituent sensitive. This behavior contrasts with that of free-base corroles and porphyrins and of

typical metalloporphyrins. We qualitatively assign this substituent sensitive transition to a ligand-to-metal charge transfer.

5. The optical spectra of the Fe(IV) and Mn(IV) corrole chloride complexes are considerably red-shifted and exhibit "hyperporphyrin" character, relative to those of the Fe(IV) corrole μ -oxo dimers. This is somewhat of a novelty compared to Fe(IV)-oxo porphyrins such as peroxidase compound II analogues and their synthetic models, but is a feature shared by chloroperoxidase compound II.¹⁷ On the basis of these developments, an interesting possibility to consider is that CPO-II may not be a high-valent oxo intermediate at all but rather an iron(IV)-hydroxy species.

Acknowledgment. We acknowledge financial support from the Norwegian Research Council and the VISTA program of Statoil, Norway. A.G. acknowledges a Senior Fellowship from the San Diego Supercomputer Center.

Supporting Information Available: The NMR spectra and a discussion of the proposed assignments. This material is available free of charge via the Internet at <http://pubs.acs.org>.

References and Notes

- Groves, J. T.; Shalyshev, K.; Lee, J. In *The Porphyrin Handbook*; Kadish, K. M., Smith, K. M., Guilard, R., Eds.; Academic: San Diego, 2000, Vol. 4, Ch. 27, 17.
- (a) Green, M. T. *J. Am. Chem. Soc.* **2000**, *122*, 9495. (b) Green, M. T. *J. Am. Chem. Soc.* **1999**, *121*, 7939. (c) Green, M. T. *J. Am. Chem. Soc.* **1998**, *120*, 10 772. (d) Green, M. T. *J. Am. Chem. Soc.* **2001**, *123*, 9218.
- Vogel, E.; Will, S.; Schulze Tilling, A.; Neumann, L.; Lex, J.; Bill, E.; Trautwein, A. X.; Wieghardt, K. *Angew. Chem., Int. Ed. Engl.* **1994**, *33*, 731. Vogel, E.; Will, S.; Schulze Tilling, A.; Neumann, L.; Lex, J.; Bill, E.; Trautwein, A. X.; Wieghardt, K. *Angew. Chem.* **1994**, *106*, 771.
- For recent reviews on the chemistry of corroles, see: (a) Paolesse, R., In *The Porphyrin Handbook*; Kadish, K. M., Smith, K. M., Guilard, R., Eds.; Academic: San Diego, **2000**, Vol. 2, Ch. 11, 201. (b) Erben, C.; Will, S.; Kadish, K. M., In *The Porphyrin Handbook*; Kadish, K. M., Smith, K. M., Guilard, R., Eds.; Academic: San Diego, **2000**, Vol. 2, Ch. 12, 233. (c) Gross, Z. *J. Biol. Inorg. Chem.* **2001**, *6*, 733. (d) Ghosh, A.; Steene, E. *J. Biol. Inorg. Chem.* **2001**, *6*, 739.
- (a) Gross, Z.; Golubkov, G.; Simkhovich, L. *Angew. Chem., Int. Ed. Engl.* **2000**, *39*, 4045. (b) Bendix, J.; Gray, H. B.; Golubkov, G.; Gross, Z. *Chem. Comm.* **2000**, 1957. (c) Golubkov, G.; Bendix, J.; Gray, H. B.; Mahammed, A.; Goldberg, I.; DiBilio, A. J.; Gross, Z. *Angew. Chem. Int. Ed. Engl.* **2001**, *40*, 2132.
- (a) Vangberg, T.; Ghosh, A. *J. Am. Chem. Soc.* **1999**, *121*, 12 154. (b) Ghosh, A.; Wondimagegn, T.; Gonzalez, E.; Halvorsen, I. *J. Inorg. Biochem.* **2000**, *78*, 79. (c) Ghosh, A.; Gonzalez, E. *Israel J. Chem.* **2000**, *40*, 1. (d) Ghosh, A.; Gonzalez, E.; Vangberg, T.; Taylor, P. *J. Porphyrins Phthalocyanines* **2001**, *5*, 345.
- Gross, Z.; Galili, N.; Simkhovich, L.; Saltsman, I.; Botoshansky, M.; Bläser, D.; Boese, R.; Goldberg, I. *Org. Lett.* **1999**, *1*, 599.
- Halvorsen, I.; Wondimagegn, T.; Ghosh, A. *J. Am. Chem. Soc.*, Submitted for publications.
- Two doublets on top of each other, based on COSY.
- The ADF program system was obtained from Scientific Computing and Modeling, Department of Theoretical Chemistry, Vrije Universiteit, 1081 HV Amsterdam, The Netherlands. For details of basis sets, grids for numerical integration, etc., the reader is referred to the program manual obtainable from this source.
- Halvorsen, I.; Ghosh, A., Unpublished results.
- Cai, S.; Walker, F. A.; Licocchia, S. *Inorg. Chem.* **2000**, *39*, 3466.
- Halvorsen, I.; Steene, E.; Nilsen, H. J.; Kadish, K. M.; Ghosh, A., Unpublished results.
- (a) Ghosh, A.; Wondimagegn, T.; Parusel, A. B. *J. Am. Chem. Soc.* **2000**, *122*, 5100. (b) Bendix, J.; Dmochowski, I. J.; Gray, H. B.; Mahammed, A.; Simkhovich, L.; Gross, Z. *Angew. Chem. Int. Ed.* **2000**, *39*, 4048.
- (a) Gans, P.; Buisson, G.; Duée, E.; Machon, J.-C.; Erler, B. S.; Scholz, W. F.; Reed, C. A. *J. Am. Chem. Soc.* **1986**, *108*, 1223. (b) Erler, B. S.; Scholz, W. F.; Lee, Y. J.; Scheidt, W. R.; Reed, C. A. *J. Am. Chem. Soc.* **1987**, *109*, 2644. (c) Schulz, C. E.; Song, H.; Mislankar, A.; Orosz, R. D.; Reed, C. A. *Inorg. Chem.* **1997**, *36*, 406.
- (a) Dawson, J. H.; Sono, M.; Eble, K. S.; Hager, L. P. *Rev. Port. Quim.* **1985**, *27*, 205. (b) Nakajima, R.; Yamazaki, I.; Griffith, B. W. *Biochem. Biophys. Res. Commun.* **1985**, *128*, 1. (c) Egawa, T.; Proshlyakov, D. A.; Miki, H.; Makino, R.; Ogura, T.; Kitagawa, T.; Ishimura, Y. *J. Biol. Inorg. Chem.* **2001**, *6*, 46–54.
- The location of the radical in CPO-I is a controversial issue. Thus, Turner et al. provided resonance Raman evidence that CPO-I may be best described as an A_{1u} -type porphyrin π -cation radical (Hosten, C. M.; Sullivan, a. M.; Palaniappan, V.; Fitzgerald, M. M.; Turner, J. *J. Biol. Chem.* **1994**, *269*, 13966). Green's^{2b} recent DFT calculations on CPO-I revealed a radical that was substantially centered on the axial thiolate ligand. Even more recently, Shaik and coworkers (Ogliaro, F.; de Visser, S. P.; Groves, J. T.; Shaik, S. *Angew. Chem. Int. Ed.* **2001**, *40*, 2874) have shown that when solvent effects are accounted for in the DFT calculations in his modeling of catalase compound I^{2d} (CAT-I), one obtains a porphyrin π -cation radical description for CAT-I only when the proximal charge relay system consisting of hydrogen bonding interactions involving the axial tyrosinate ligand is accounted for in the calculations. Otherwise, one obtains a description involving an iron(IV)-oxo porphyrin with an axial tyrosinate radical.